Terminal reflections in fiber-optic image guides

Pierre M. Lane

Cancer Imaging Department, British Columbia Cancer Research Center, 675 West 10 Avenue, Vancouver, BC V5V 1L3, Canada (plane@bccrc.ca)

Received 15 June 2009; revised 25 September 2009; accepted 25 September 2009; posted 1 October 2009 (Doc. ID 112787); published 16 October 2009

Fibered image guides for confocal reflectance endomicroscopy suffer from Fresnel reflections at the fiber terminals, which can limit signal-to-noise ratio in these systems. A model that describes these terminal reflections is presented to better understand how they can be managed most effectively. An expression for the refractive index of termination that minimizes the reflection as a function of the fiber's normalized frequency is derived for step-index fibers, while a graphical solution is presented for graded-index fibers. The model predicts that terminal reflections from graded-index fibers are more sensitive to variations in fiber size and changes in wavelength than step-index fibers. A method is also presented to measure the refractive index that allows one to minimize the terminal reflections in an image guide. The technique uses the inherent mode coupling of the fibers in the image guide, allowing the isolation and measurement of reflections from only one end of the fiber. An achievable minimum backreflection of −36 dB was measured at 635 nm in a commercial image guide with 30,000 fibers.

OCIS codes: 060.2270, 060.2350, 110.2350, 120.3890, 170.2150, 170.1790.

1. Introduction

Optical image guides composed of thousands of optical fibers are used in many optical instruments to relay images from inaccessible or inhospitable areas. Unless an optical coupling medium is employed, there is a small Fresnel reflection as light is coupled into the fibers of the image guide and again as the light exits. Even when a refractive index (RI) coupling medium is used, it is difficult to completely attenuate these terminal reflections. The terminal reflections do not pose a problem in conventional endoscopes, laparoscopes or other instruments that employ separate illumination and imaging pathways. Confocal instruments that employ a fiber-optic image guide [1] use the fibers in a bidirectional mode for both illumination and detection and, as a consequence, the contrast of these instruments can be limited by terminal reflections from the image guide.

Image contrast in fiber-optic confocal instruments is generated through either reflectance or fluorescence [2,3]. In fluorescence-contrast systems [4,5], the illumination (excitation) and detection (emission) light are separated in wavelength so the backreflected illumination light is easily attenuated using an appropriate long-pass filter. Attenuation of backreflected light in a reflection-contrast system is more difficult. Contrast in tissue reflectance imaging is generated by microscopic RI variations in the tissue [6]. A simple reflectance calculation based on RI data alone (ignoring the scattering effects that would reduce contrast even further) reveals that the backscatter contrast due to melanin [7] is −20 dB relative to the incident light and that due to amelanotic tissue [8,9] is −35 dB. The signal-to-noise ratio implications for these confocal systems become clear when one considers that the minimum image-guide backscatter is of the same order of magnitude (minimum terminal reflection of −36 dB measured at 635 nm in this study).

As evidenced by studies involving conventional (as opposed to fiber-optic) confocal microscopy of surgical specimens, both fluorescence [10,11] and reflection [7,12–14] contrast provide imagery that can be used for disease diagnosis. Fibered image-guide systems for confocal fluorescence endomicroscopy have been deployed for pilot clinical trials by several research groups [15,16] and a commercial system is available from Mauna Kea Technologies (Paris, France). Even

0003-6935/09/305802-09$15.00/0

though reflection contrast can provide diagnostic imagery, there have been few devices reported in the literature [17] and currently no systems are available commercially. The reason for this is likely the technical challenges involved in achieving sufficient reflection contrast due to terminal reflections.

The problem of terminal reflections in an image guide is illustrated in Figure 1. The figure shows a fiber-optic image guide (Schott LB5567) with step-index fibers hexagonally packed on 8.5 μm centers. The fibers are illuminated for reflectance contrast and terminated with oils of different RI. As shown in the top-left panel (*), the terminal RI $n_0 = 1.49$ matches that of the cladding and only the cores scatter incident light. Similarly, in the bottom row (**), the terminal RI $n_0 = 1.62$ matches that of the cores. As illustrated, RI matching to minimize terminal reflections would appear to be straight forward, however, most high density image guides used in practical devices employ graded-index fibers rather that the step-index fibers illustrated. As one might expect, the task of RI matching becomes more difficult in graded-index fibers where it is not possible to index match the entire fiber core, and, as will be shown, variations in fiber size, shape, and wavelength lead to variations in the optimum RI for index matching.

In this paper a model of terminal reflections in step and graded-index fibers is derived and a method is proposed to measure the optimum RI of a terminating medium to minimize these backreflections under given operating conditions. In addition to RI matching, there are other common techniques available to reduce terminal reflections; however, most are not applicable to image guides. For example, return loss in telecom fibers is kept below −60 dB by using angle polished connectors (APCs) that incorporate a polished face at an 8° angle to redirect the reflection into the cladding. Although this principle could be applied to images guides, their large diameter and NA necessitates large polishing angles and further complicates the design of the downstream optics. Other techniques include a time or coherence gate to remove the unwanted reflections, masking the cladding region of the fibers [18], or attenuation of the reflections during image post processing [19].

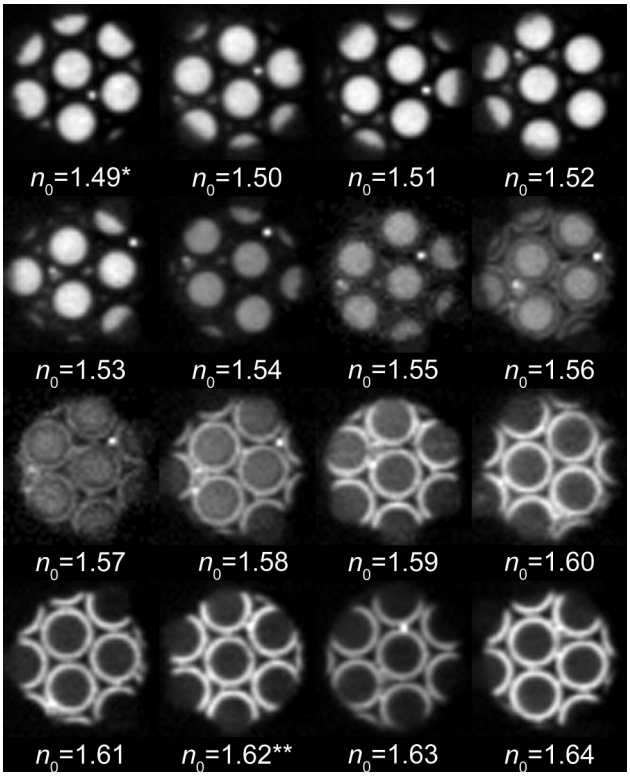

Fig. 1. Terminal backreflections from a fiber-optic image guide terminated with oils of different RI, n_0. The image guide (Schott LB5567) has step-index fibers hexagonally packed with an 8.5 μm center-to-center pitch. The terminal RI matches that of the cladding at $n_0 = 1.49$ (top left, *) and that of the core at $n_0 = 1.62$ (bottom row, **).

In the first half of this paper a model of terminal Fresnel reflections from the fibers of an image guide is derived. A general expression for the terminal backreflection as a function of termination RI is derived and special cases are derived for step and graded-index fibers. An expression for the terminal RI that minimizes the backreflection as a function of the fiber's normalized frequency is derived for the step-index case while a graphical solution is presented for the graded-index case. In the second half a novel method is presented to measure the RI that minimizes terminal reflections in an image guide. Measured backreflection data as a function of termination RI for a Sumitomo image guide are reported.

2. Terminal Reflection Model

The symbols used in the termination model are defined schematically in Fig. 2. Three fibers from an image guide are represented in the figure as the shaded regions. The terminal RI, n_0, is constant while the RI in each fiber, $n(r)$, has a radial dependence parameterized by the core RI, n_1, and cladding RI, n_2. Complex amplitude U_1 is the guided field of the central fiber moving toward the terminal interface (down). Complex amplitude U_2 is the reflected part of U_1 after reflection from the terminal interface. It is assumed that U_1 and U_2 represent the complex amplitudes near the interface and that the guided modes are free to couple into other fibers as they propagate along the fiber farther away from the interface.

It is also assumed that most of the optical power is coupled into the fiber's fundamental mode. This assumption is typically valid in practice where a Gaussian beam is launched into the fibers of the light guide. The complex amplitude of the propagating field U_1 is, therefore, defined as a fundamental mode with a Gaussian amplitude distribution,

$$U_1(r) = \sqrt{I_0}\exp\left(-\frac{r^2}{w_0^2}\right), \tag{1}$$

where I_0 is the optical intensity of the field, r is the radial dimension of the fiber, and w_0 is the Gaussian waist radius of the mode. The complex amplitude

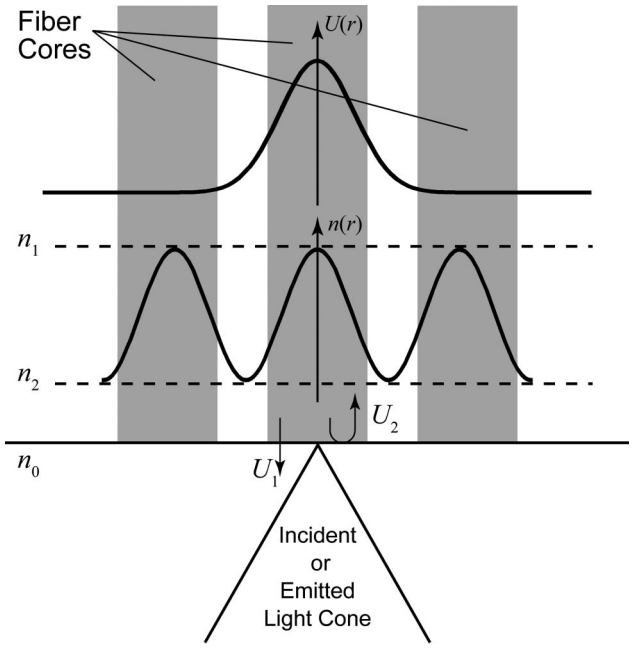

Fig. 2. Schematic illustrating the symbols used in the termination model. The terminal RI, n_0, is constant while the RI in each fiber, $n(r)$, has radial dependence parameterized by the core RI, n_1, and cladding RI, n_2.

of the field reflected by the terminal interface is efined by

$$U_2(r) = \rho\left[n\left(\frac{r}{a}\right), n_0\right] U_1(r), \tag{2}$$

and the amplitude reflectance function is

$$\rho(\eta_1, \eta_2) = \frac{\eta_1 - \eta_2}{\eta_1 + \eta_2}, \tag{3}$$

where η_1 and η_2 are refractive indices on the incident and transmitted sides of the interface, respectively, and n_0 is the RI of the termination medium. The amplitude reflectance function assumes that the angle of incidence is small (almost normal incidence). This assumption is valid in practice as typically the marginal rays are incident to the fiber at less than 20° and the Fresnel equations are relatively insensitive to angle when the angle is small. This assumption greatly simplifies the analysis as there is no distinction between TE and TM polarizations.

Fiber backreflection is defined as

$$\mathcal{R}(n_0) = \mathcal{R}_{\text{term}}(U_1, U_2)\eta(U_1, U_2), \tag{4}$$

which is the fraction of optical power propagating in the fiber that is reflected at the terminal interface and then recoupled back into the same fiber propagating in the opposite direction. The first term, defined by,

$$\mathcal{R}_{\text{term}}(U_1, U_2) = \frac{\int_0^\infty |U_2(r)|^2 r\mathrm{d}r}{\int_0^\infty |U_1(r)|^2 r\mathrm{d}r}, \tag{5}$$

describes the fraction of power reflected at the interface due to the Fresnel reflections, while the second term,

$$\eta(U_1, U_2) = \frac{\left|\int_0^\infty U_1(r)\bar{U}_2(r) r\mathrm{d}r\right|^2}{\int_0^\infty |U_1(r)|^2 r\mathrm{d}r \int_0^\infty |U_2(r)|^2 r\mathrm{d}r}, \tag{6}$$

accounts for the recoupling of the reflected power back into the fiber. Equation (6) is the normalized overlap integral between the spatial distribution of the fiber's fundamental mode, U_1, and the reflected wavefront amplitude incident on the fiber, U_2. The overbar in Eq. (6) indicates complex conjugation and the overlap integral in the numerator allows for the normalization against the incident and guided optical powers.

An expression for fiber backreflection is obtained as a function of terminal RI, n_0, by substituting the reflection and recoupling expressions [Eqs. (5) and (6)] and the expressions for the guided and reflected complex amplitudes [Eqs. (1)–(3)] into Eq. (4),

$$\mathcal{R}(n_0) = \left(\frac{2}{w_0}\right)^4 \left[\int_0^\infty \exp\left(\frac{-2r^2}{w_0^2}\right) \frac{n_0 - n\left(\frac{r}{a}\right)}{n_0 + n\left(\frac{r}{a}\right)} r\mathrm{d}r\right]^2. \tag{7}$$

The expression for backreflection is parameterized by the Gaussian radius of the mode, w_0, and the RI profile of the fiber, $n(r/a)$, where a is the radius of the fiber core. As expected, the backreflection is zero for the special case when $n(r/a) = n_0$.

In Subsections 2.A and 2.B, the specific cases of step and graded-index fibers are considered to determine the terminal RI that minimizes backreflection. The step-index fiber has a simple analytic solution for minimum backreflection but unfortunately this does not apply to typical image guides, which employ graded-index fibers. The graded-index solution is more complicated and a graphical solution is presented.

A. Step-Index Profile

Consider now the approximate Gaussian solution to the scalar wave equation for a circular waveguide with a step-index RI profile defined by

$$n(R) = \begin{cases} n_1, & r \le 1 \quad (\text{core}) \\ n_2, & r > 1 \quad (\text{clad}) \end{cases}, \tag{8}$$

where $R = r/a$ has been introduced as the radial coordinate normalized to the fiber core radius and $W_0 = w_0/a$ as the normalized Gaussian radius. Under the Gaussian approximation [20], the field distribution of the fundamental mode for the step-index profile defined by Eq. (8) is given by the Gaussian of Eq. (1) with a normalized Gaussian radius defined by

$$W_0 = (\ln V)^{-\frac{1}{2}}, \tag{9}$$

where $V = 2\pi(a/\lambda)(n_1^2 - n_2^2)^{1/2}$ is the normalized frequency of the fiber. The normalized frequency is used

here to describe the confinement of the fundamental mode in the fiber and its dependence on wavelength.

Substitution of Eqs. (8) and (9) into Eq. (7) yields an expression for the backreflection in a step-index fiber,

$$\mathcal{R}_{\text{step}}(n_0) = \frac{1}{V^4}\left[\left(\frac{n_2 - n_0}{n_2 + n_0}\right)^2 + (V^2 - 1)^2\left(\frac{n_2 - n_0}{n_2 + n_0}\right)^2\right]. \quad (10)$$

The first and second terms in Eq. (10) go to zero when the terminal RI matches that of the cladding and core, respectively. In the limit, as V approaches 1 (the guided mode becomes less confined to the core), the second term goes to zero and the backreflection is determined by the difference between the cladding and terminal refractive indices.

An expression for the terminal reflective index that minimizes Eq. (10) can be derived analytically; however, the solution is quite cumbersome. The first-order approximation to the solution is

$$N_0^{\text{step}} = 1 - \frac{\Delta}{2 - 2V^2 + V^4}, \quad (11)$$

where $\Delta = (n_1^2 - n_2^2)/2n_1^2$ is the RI contrast of the fiber, and the normalized terminal RI is given by $N_0 = n_0/n_1$. The error introduced in Eq. (11) by the approximation is much less than 1% for $\Delta < 0.05$ and $V > 1$.

B. Graded-Index Profile

Now consider the approximate Gaussian solution for a circular waveguide with a Gaussian RI profile defined by

$$n(R) = n_1\sqrt{1 - 2\Delta[1 - \exp(-R^2)]}. \quad (12)$$

The profile decreases gradually from n_1 to n_2 as R increases from 0 to ∞ and leads to a simple Gaussian approximation of the field distribution [20]. While the infinite parabolic RI profile also leads to a Gaussian solution of the scalar wave equation, its profile decreases to $-\infty$ as R goes to ∞ leading to numerical instabilities during integration over R. The field distribution of the fundamental mode for the step-index profile defined by Eq. (12) is given by the Gaussian of Eq. (1) with a normalized Gaussian radius defined by

$$W_0 = \sqrt{\frac{2}{V - 1}}. \quad (13)$$

This expression is physically meaningful when $V > 1$, however, most cases of practical interest when the fundamental mode is reasonably confined to the core satisfy this condition. Substitution of Eq. (13) into Eq. (7) yields an expression for the backreflection in a graded-index fiber with Gaussian RI profile:

$$\mathcal{R}_{\text{Gauss}}(n_0) = 4(V - 1)^2 \times \left[\int_0^\infty \exp[-(V - 1)R^2]\rho(R)R\,dR\right]^2, \quad (14)$$

where

$$\rho(R) = \frac{N(R) - N_0}{n(R) + N_0} \quad (15)$$

is the amplitude reflectivity, $N(R) = n(R)/n_1$ is the normalized RI profile, and $n(R)$ is the Gaussian RI profile defined by Eq. (12).

The normalized RI profile $N(R)$ and the power reflectance $|\rho(R)|^2$ for a typical image-guide fiber with $\Delta = 3.16\%$ are plotted in Fig. 3. The dashed horizontal lines indicate the normalized terminal (upper) and cladding (lower) refractive indices. As shown, the power reflectance goes to zero at $R = R_0$ for $N_0 = 0.995$ where the RI of the graded-index profile matches that of the termination medium. The incident (U_1) and reflected (U_2) field amplitudes are shown in Fig. 4 for a fiber with $V = 7$. As shown, for $R > R_0$, the field experiences an external reflection [$n_0 > n(R)$] and the wavefront undergoes a phase shift. The backreflection defined by Eq. (14) can, in principle, be completely attenuated if N_0 is chosen such that it divides the regions of internal and external reflectance so the area under the curve is zero. This is a consequence of the definition of backreflection being the integral of reflected amplitude squared rather than the integral of reflected power as would have be the case if one did not consider recouping of the reflected field.

Backreflection as a function of normalized terminal RI for different normalized frequencies is plotted in Fig. 5. Normalized frequency describes the confinement of modes propagating in the fiber (larger V means tighter confinement) and, therefore, strongly influences backreflection as the width of the wavefront scales inversely with V while the RI profile is fixed. In the limit, as the mode becomes completely confined to the core, the normalized terminal RI that minimizes backreflection approaches 1.

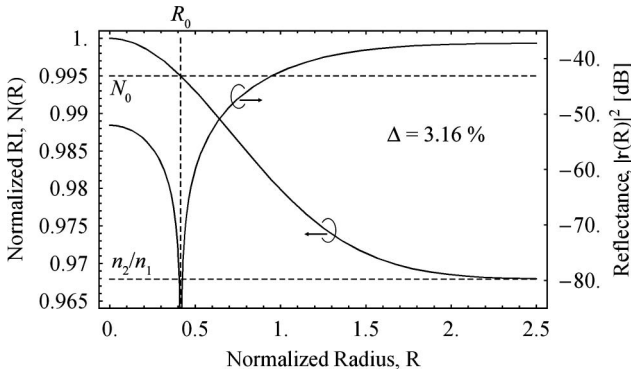

Fig. 3. Normalized RI and reflectance as a function of normalized radius for a graded-index fiber with a Gaussian RI profile. The normalized terminal RI is N_0.

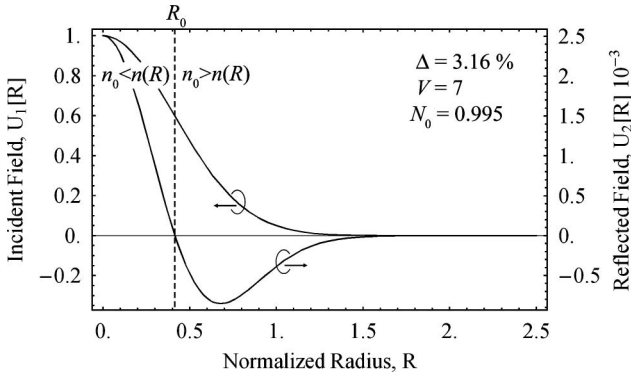

Fig. 4. Incident and reflected field amplitudes as a function of normalized radius for a graded-index fiber with a Gaussian RI profile and a terminal reflective index of $N_0 = 0.995$. When $R > R_0$, the incident wave function undergoes an external reflection and experiences a phase shift on reflection.

Finally, the normalized terminal RI than minimizes backreflection in a graded-index fiber is shown graphically as a function of normalized frequency. Figure 6 shows the normalized terminal refractive indices required to minimize backreflection and normalized spot size versus normalized frequency. The shaded region indicates the normalized frequency of an image guide with 3 μm diameter cores operating in wavelength ranges from 400 nm ($V = 1.8$) to 2 μm ($V = 8.9$). Single-mode cutoff is at $V = 2.405$ and the dashed line indicates the conditions for minimum terminal reflection at 635 nm ($V = 5.6$). The normalized terminal RI required to minimize backreflection in a step-index fiber [Eq. (11)] is shown for comparison (dashed curve).

3. Termination for Minimum Backreflection

Here a method is presented to measure the terminal RI that minimizes the backreflection in a commercial image guide. Only basic specifications are provided by the manufactures for their image guides, making it very difficult to validate the model from the Section 2 without measuring the RI profile directly.

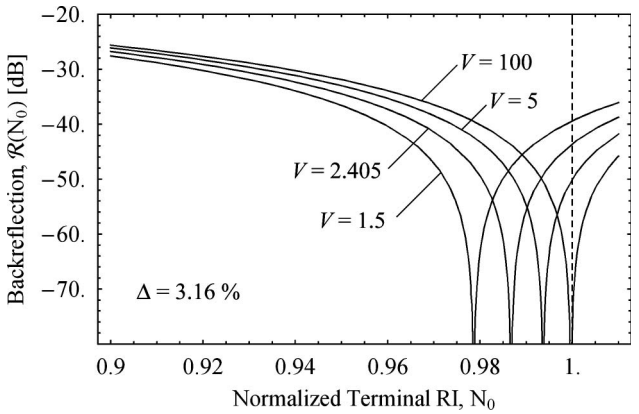

Fig. 5. Terminal reflections as a function of normalized terminal RI for different normalized frequencies. At large normalized frequencies, the fundamental mode is tightly confined and the terminal RI that minimizes the terminal reflection is equal to the core RI ($N_0 = 1$).

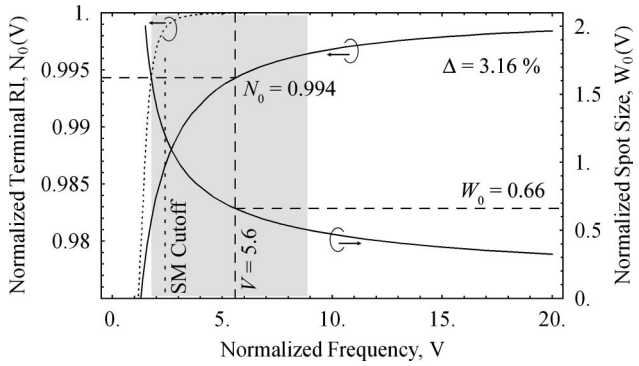

Fig. 6. Normalized terminal refractive indices required to minimize the backreflection and normalized spot size versus normalized frequency. The shaded region indicates the normalized frequency of an image guide with 3 μm diameter cores operating in wavelength ranges from 400 nm ($V = 1.8$) to 2 μm ($V = 8.9$). Single-mode cutoff is at $V = 2.405$, and the dashed line shows the conditions for minimum terminal reflection at 635 nm. The normalized terminal RI required to minimize the terminal backreflection for a step-index fiber is shown for comparison (dashed curve).

Further complicating model validation is the manufacture's definition of core RI and whether it is defined as the maximum on-axis RI of the fiber (as used here) or as an effective value averaged over the fiber core. In addition, there is a large variability in the shape [21,22] and RI profile [23] of the fibers, further complicating the measurement of theses parameters. Direct comparison with the model would therefore need to be done on a fiber-by-fiber basis rather than using averaged parameters from a population of fibers.

For these reasons, the terminal RI that minimizes backreflection for a small number of fibers within a bundle is measured. An exact comparison with published image-guide specifications is not possible; however, the model presented in Section 2 serves to explain the process, and ultimately, it is the terminal RI that is of primary importance rather than a detailed characterization of the RI profile.

A. Measurement Model

A common technique used to measure the backreflection due to RI mismatch is to measure the light reflected back from the input end of a fiber while the output end is terminated for effectively zero backreflections. This method is employed by backreflection meters for telecom applications where it is easy to achieve backreflections better than −60 dB from APC connectors, a mandrel wrap, or a RI matching fluid. These termination methods are not applicable to image guides that have a large NA and are mechanically stiff. In particular, the optimal RI matching fluid is not known *a priori* and, unlike a step-index telecom fiber, the RI that minimizes backreflection in a graded index, as shown, is sensitive to fiber geometry and wavelength. For these reasons, a new technique to measure backreflection was developed that takes advantage of the inherent mode

coupling of the image guide to relax the requirements of fiber termination.

Light is launched into one fiber and the reflected light returning along an adjacent fiber is measured to avoid the terminal reflection going into the fiber. This technique is illustrated schematically in Fig. 7. Light launched into fiber 1 from the microscope objective lens is partially coupled into fiber 2 due to mode coupling [21] as it propagates along the length of the light guide. Light from fiber 2 undergoes a reflection at the distal end and is guided back to the proximal end where its intensity is measured. Because the reflection due to launching light into the light guide (fiber 1) is spatially separated from the reflection due to light leaving the light guide (fiber 2), only the reflectance from the distal end of the fiber is measured.

This offers two significant advantages. First, measurement of the terminal reflection from the distal end can be isolated from the reflection at the proximal end. Second, from an experimental point of view, it is much easier to change the RI oil at the distal end as opposed to changing it at the proximal end, where each RI oil change necessitates that the fiber be defocused, cleaned, and refocused to change the oil. This is difficult to do without accidently translating or rotating the image guide even slightly, making it impractical (time consuming) to recouple light into the same fiber.

The terminal backreflection is assumed to be described by a power reflectance function plus a constant reflectance offset as follows:

$$\mathcal{R}_{12}(n_0) = \frac{I_{2r}}{I_1} = 2\kappa_{12}\left[\left(\frac{n_{\text{eff}} - n_0}{n_{\text{eff}} + n_0}\right)^2 + \mathcal{R}_0\right]. \quad (16)$$

The functional form and shape of this equation are similar to those presented earlier [Eqs. (7), (10), and (14)]; however, here the normalized frequency and RI profile are wrapped into an effective RI parameter, n_{eff}, which is a function of fiber geometry and wavelength. Our group has shown that the constant backreflection term $\mathcal{R}_0$ is due to Rayleigh scatter along the length of the fiber and has a λ^{-4} wavelength dependence [24]. The third parameter in Eq. (16), κ_{12}, is the power-coupling coefficient illustrated schematically in Fig. 7. The factor of two is due to the measurement of identical reflections from both fibers. Higher-order interactions due to multiple coupling between fibers are assumed to be negligible.

B. Materials and Methods

The setup used to measure backreflection is illustrated schematically in Fig. 8. Light from a single-mode fiber pigtailed 635 nm laser diode was coupled exclusively into one fiber of the image guide under test. A seven-times relay system composed of a fiber port (Thor Labs, p/n PAF-X-18-PC-B) and microscope objective lens (Zeiss 63X/1.4) coupled light from the fiber pigtail (Fibercore, SM600) onto the input face of the image guide. The mode-field diameter (MFD) of the fiber pigtail projected onto the image guide was 0.8 μm. A 50/50 beam splitter in the path between the fiber port and the objective lens allowed for the inspection of the image guide using a tube lens and

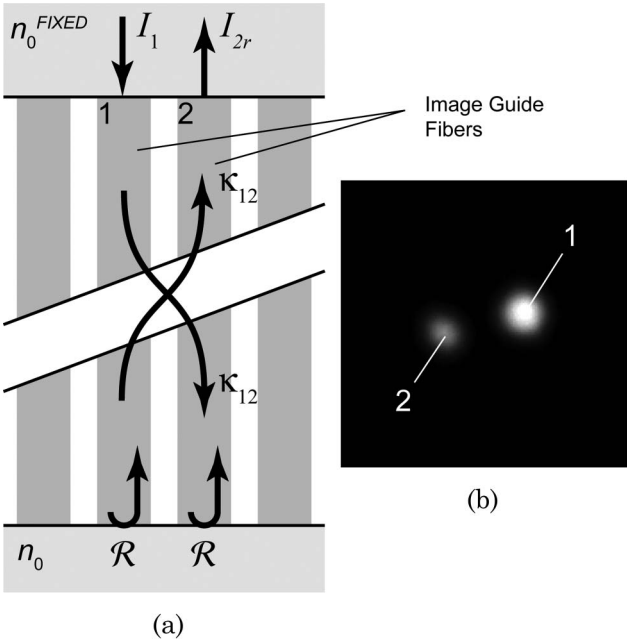

Fig. 7. Schematic illustration of mode coupling between two fibers in an optical image guide: (a) Light coupled into fiber 1 from the microscope objective lens is partially coupled into fiber 2 due to mode coupling along the length of the fiber. Light measured from fiber 2 is due to a reflection from the distal end only. (b) Image intensity distributions measured from fibers 1 and 2.

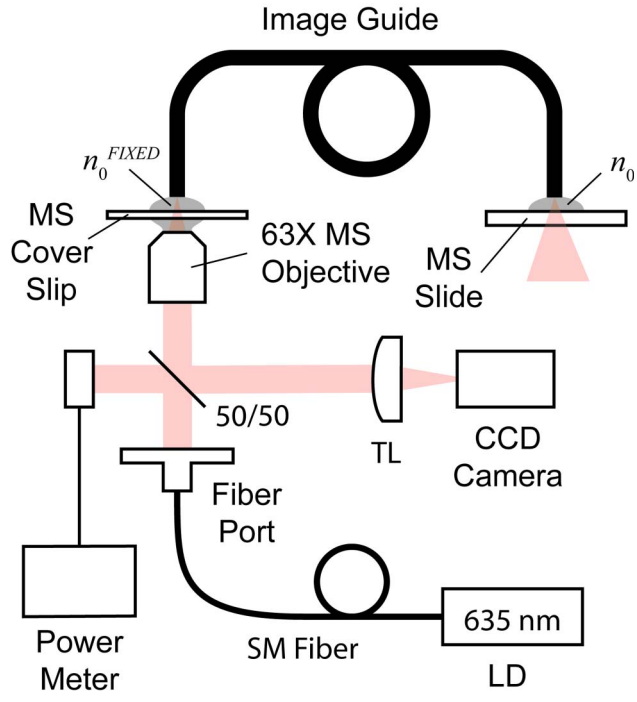

Fig. 8. (Color online) Schematic illustration of the experimental setup used to measure terminal reflection as a function of terminal RI: microscope (MS), laser diode (LD), tube lens (TL), single-mode (SM), charge coupled device (CCD).

CCD camera. Back-illumination of the image guide enabled targeting of individual fibers by translating the image guide while viewing the image of the laser spot on the back-illuminated image guide. A power meter measured the reference power reflected from the 50/50 beam splitter.

The objective lens was optically coupled to the image guide using a (fixed) RI matching fluid, and the opposite end of the image guide was coupled into a tilted microscope side using a (variable) RI matching fluid. The fixed RI matching fluid is used to optically couple light to and from the image guide, while the variable RI matching fluid is varied to affect a change in the signal backreflected from light exiting the image guide.

The variation of backreflection from three fibers in two Sumitomo images guides (IGN-08/30) was measured. The light guides were measured as-shipped from Sumitomo and were not cut or repolished. The RI oil used to couple the microscope objective to the image guide was fixed at $n_0^{\mathrm{FIXED}} = 1.500$. The RI oil at the opposite end of the light guide was varied and the resulting backreflection was measured. The following RI values were used: 1.000, 1.330, 1.440, 1.460, 1.480, 1.500, 1.520, 1.540, 1.560, 1.580, and 1.600. The first and second RI media were air and water, respectively, while the remainder was RI oils from Cargille Laboratories (Cedar Grove, New Jersey). The RI oils were specified at 589.1 nm and 25 °C with a tolerance of ±0.0002.

Light was coupled into a single fiber by translating the light guide with respect to the microscope objective lens and monitoring the alignment using the CCD camera. Illumination-detection fiber pairs (fibers 1 and 2 in Fig. 7) were chosen that coupled strongly to maximize the signal detected. The end of the fiber proximal to the microscope objective was fixed for the remainder of the experiment after the illumination fiber was selected and focused. The coupling medium at the distal end was replaced in sequence and a CCD image of the illumination-detection fiber pair was recorded for each RI value. The image guide and microscope slide were cleaned with xylene between each step to avoid mixing the oils. The complete sequence of 11 RI values was measured three times and a mean and standard deviation was calculated for each.

The CCD images were processed to measure the intensity returned by the detection fiber. The intensity was calculated as the sum of background-corrected pixels corresponding to the fiber core. The intensity was normalized by the laser power detected by the power meter to account for variations in laser power. Finally, the set of 11 intensity measurements were referenced to the intensity produced by a mirror of known reflectance when measured in the same manner. The mirror was focused and coupled to the microscope objective in a manner identical to the image guide. The dataset was fit to the model of Eq. (16) using a nonlinear least-squares fit based on the Levenberg–Marquardt algorithm.

C. Results

Measured reflectance data and least-squares fits are plotted in Fig. 9. Reflectance data from the single fiber core measured in the first image guide (core 1) are shown in part (a), while that from the two fiber cores measured in the second image guide (cores 2 and 3) are shown in part (b). The error bars represent the standard deviation of three replicate measurements. Best-fit estimates and 95% confidence intervals for the three parameters (κ_{12}, n_{eff}, and $\mathcal{R}_0$) and the goodness of fit (R^2) for the three cores are presented in Table 1.

4. Discussion

The model is a good fit to the measured data as shown in Fig. 9 as evidenced by the high values for goodness of fit in Table 1. One of the best-fit estimates for the RI that minimized the terminal reflection appears to be different from the other two. A Student's t test was used to compare the best-fit values for n_{eff} from the three experiments. The value for core 2 was not statistically different from the other two cores; however, core 1 was significantly different from core 3 ($P = 0.05$). The difference between cores is consistent with the observation that the size and shape of the cores varies in an image guide. Because terminal reflections are sensitive to fiber shape

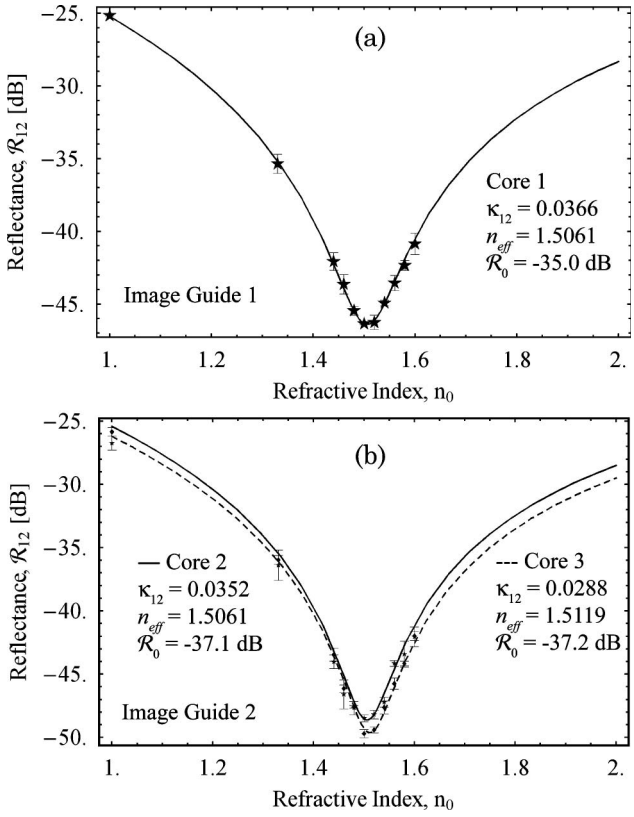

Fig. 9. Measured terminal reflectance versus terminal RI for two different fiber-optic image guides: Reflectance data from (a) a single fiber core from the first image guide and (b) two fiber cores in the same image guide. The curves are nonlinear least-squares fits to the data points, and the best-fit parameters are indicated.

Table 1. Nonlinear Least-Squares Fit Results[a]

	$\hat{n}_{\text{eff}}$		$\hat{\kappa}_{12}$		$\hat{\mathscr{R}}_0$[dB]		
	Est ± SE	95% CI	Est ± SE	95% CI	Est ± SE	95% CI	R^2
Core 1	1.5061 ± 0.0013	(1.5031, 1.5090)	0.0366 ± 0.0003	(0.0359, 0.0372)	−35.0 ± 0.1	(−35.2, −34.9)	0.9997
Core 2	1.5061 ± 0.0028	(1.4996, 1.5127)	0.0352 ± 0.0036	(0.0270, 0.0435)	−37.1 ± 0.6	(−40.0, −35.8)	0.9800
Core 3	1.5119 ± 0.0011	(1.5094, 1.5144)	0.0288 ± 0.0013	(0.0258, 0.0318)	−37.2 ± 0.3	(−38.1, −36.5)	0.9970
Average	1.5080 ± 0.0011		0.0335 ± 0.0013		−36.4 ± 0.2		

[a]SE, standard error; CI, confidence interval.

and wavelength, as shown in Figs. 5 and 6 through the normalized frequency parameter, one would also expect n_{eff} to be sensitive to fiber size, shape, and wavelength. It is not practical to individually match the RI of each fiber core to achieve a minimum reflection; however, it is possible to minimize the average reflection of all fiber cores taken as a whole at a particular wavelength. For the measurements reported here, the average of the three best-fit estimates for the RI that minimized the terminal reflection at 635 nm was $n_{\text{eff}} = 1.508 \pm 0.001$. Data from Sumitomo [25] on RI specified an average core RI of 1.49 (1.50 on axis) and a cladding RI of 1.45; however, it was not clear how these measurements were made.

A similar comparison using the Student's t test was completed between the minimum reflection parameter $\mathscr{R}_0$ for each core measurement. The minimum reflectance for core 2 was not statistically different from core 3, however, there was a significant difference between core 1 and the other two cores ($P = 0.05$). Our group has shown than the minimum reflectance from fibers in an image guide is due to Rayleigh scattering [24]. Although the intensity of Rayleigh scattered light is primarily dependent on wavelength, there may also be a fiber size and shape dependence. The portion of the wavefront propagating close to the fiber axis, where the Ge doping is typically quite high in Sumitomo and Fujikura image guides, Rayleigh scatters more than the portion of the field propagating far from the axis. One would therefore expect more Rayleigh scatter for highly confined modes associated with small normalized frequencies. The size differences between fibers (and the corresponding variation in V) may therefore have a measurable effect on Rayleigh backscatter. The average of the three best-fit estimates for minimum backreflection at 635 nm was $\mathscr{R}_0 = -36.4 \pm 0.2$ [dB].

Crosstalk in image guides due to mode coupling is well documented [22,26,27]. Reichenbach and Xu recently showed that the subtle nonuniformities in fiber size reduces mode coupling between fibers in an image guide [21] and, in fact, the variations in fiber size and shape are required for the transmission of high resolution imagery in a fiber-optic light guide.

The best-fit parameter measured for power coupling (κ_{12}) ranged between 3 and 4% and is consistent with values reported by Chen *et al.* [22]. The crosstalk estimated here is typical of the maximum value for the image guide because fiber pairs with large coupling were located to increase the signal-to-noise ratio of the reflectance measurements. Power coupling at 635 nm was measured; however, one would expect the coupling to increase with wavelength due to decreased confinement (smaller normalized frequency) of the guided modes. Poor image quality due to increased mode coupling at longer wavelength was also noted by Chen *et al.* [22].

The terminal reflection model presented here was derived for the exit reflection of a guided mode propagating in the fiber at the distal end of an image guide. The conditions that minimize this exit reflection were determined. If light is launched into and detected from the image guide using an optical fiber, the same terminal reflection model can also be applied to the entrance reflections at the proximal end of the image guide. It was assumed that a single optical illumination and detection fiber is optically coupled by a relay system with appropriate magnification to a designated fiber in the image guide. Assuming the relay system does not introduce any optical aberrations, the Gaussian wavefront illuminating the fiber, U_1, is given by Eq. (1) where $2w_0$ is now the MFD of the illumination-detection fiber scaled by the magnification of the relay system. Similarly, the reflected wavefront, U_2, is given by Eq. (2) where, as before, a is the core radius of the image-guide fiber. This model could be used to predict the variation of the entrance reflection as it changes with the MFD of the illumination–detection fiber relative to the size of the image-guide fiber (w_0/a).

5. Conclusions

A model that describes the terminal Fresnel reflections from the fibers within an image guide was derived. The model can be applied to the exit reflections due to light leaving the image guide and to the entrance reflections due to the injection of light. A general expression for terminal backreflection as a function of terminal RI was derived and special cases were derived for step and graded-index fibers. An expression for the terminal RI that minimizes backreflection as a function of the fiber's normalized frequency was derived for the step-index case, while a graphical solution was presented for the graded-index case. The model predicted that terminal reflections from graded-index fibers (typically used in commercial image guides) are more sensitive to variations in size and shape and changes in wavelength than step-index fibers.

A method to measure the RI that minimizes terminal reflections in an image guide was also presented. The technique uses the inherent mode coupling of the fibers in the image guide, allowing for the isolation and measurement of reflections from only one end of the fiber. The terminal RI that minimizes terminal reflections should be selected (either empirically and/or theoretically) for the specific image guide and operating wavelength. As the RI that minimizes back-reflections is dependent on wavelength, owing to the variation in confinement at different normalized frequencies, image-guide characterization for the purpose of instrumentation development should be completed at the operating wavelength of the instrument.

References

1. A. F. Gmitro and D. Aziz, "Confocal microscopy through a fiberoptic imaging bundle," Opt. Lett. **18**, 565–567 (1993).
2. C. MacAulay, P. Lane, and R. Richards-Kortum, "In vivo pathology: microendoscopy as a new endoscopic imaging modality," Gastrointest. Endosc. Clin. N. Am. **14**, 595–620 (2004).
3. K. Sokolov, K. B. Sung, T. Collier, A. Clark, D. Arifler, A. Lacy, M. Descour, and R. Richards-Kortum, "Endoscopic microscopy," Dis. Markers **18**, 269–291 (2002).
4. B. A. Flusberg, E. D. Cocker, W. Piyawattanametha, J. C. Jung, E. L. M. Cheung, and M. J. Schnitzer, "Fiber-optic fluorescence imaging," Nat. Methods **2**, 941–950 (2005).
5. Y. S. Sabharwal, A. R. Rouse, L. Donaldson, M. F. Hopkins, and A. F. Gmitro, "Slit-scanning confocal microendoscope for high-resolution in vivo imaging," Appl. Opt. **38**, 7133–7144 (1999).
6. A. K. Dunn, C. Smithpeter, A. J. Welch, and R. Richards-Kortum, "Sources of contrast in confocal reflectance imaging," Appl. Opt. **35**, 3441–3446 (1996).
7. M. Rajadhyaksha, M. Grossman, D. Esterowitz, R. H. Webb, and R. R. Anderson, "In-Vivo confocal scanning laser microscopy of human skin—melanin provides strong contrast," J. Invest. Dermatol. **104**, 946–952 (1995).
8. C. Smithpeter, A. Duan, R. Drezek, T. Collier, and R. Richards-Kortum, "Near real time confocal microscopy of cultured amelanotic cells: sources of signal, contrast agents and limits of contrast," J Biomed. Opt. **3**, 429–436 (1998).
9. R. Drezek, A. Dunn, and R. Richards-Kortum, "Light scattering from cells: finite-difference time-domain simulations and goniometric measurements," Appl. Opt. **38**, 3651–3661 (1999).
10. I. Pavlova, K. Sokolov, R. Drezek, A. Malpica, M. Follen, and R. Richards-Kortum, "Microanatomical and biochemical origins of normal and precancerous cervical autofluorescence using laser-scanning fluorescence confocal microscopy," Photochem. Photobiol. **77**, 550–555 (2003).
11. E. R. Hsu, A. M. Gillenwater, M. Q. Hasan, M. D. Williams, A. K. El-Naggar, and R. R. Richards-Kortum, "Real-time detection of epidermal growth factor receptor expression in fresh oral cavity biopsies using a molecular-specific contrast agent," Int. J. Cancer **118**, 3062–3071 (2006).
12. T. Collier, A. Lacy, R. Richards-Kortum, A. Malpica, and M. Follen, "Near real-time confocal microscopy of amelanotic tissue: detection of dysplasia in ex vivo cervical tissue," Acad. Radiol. **9**, 504–512 (2002).
13. T. Collier, M. Guillaud, M. Follen, A. Malpica, and R. Richards-Kortum, "Real-time reflectance confocal microscopy: comparison of two-dimensional images and three-dimensional image stacks for detection of cervical precancer," J. Biomed. Opt. **12**, 024021 (2007).
14. A. L. Clark, A. M. Gillenwater, T. G. Collier, R. Alizadeh-Naderi, A. K. El-Naggar, and R. R. Richards-Kortum, "Confocal microscopy for real-time detection of oral cavity neoplasia," Clin. Cancer Res. **9**, 4714–4721 (2003).
15. J. A. Udovich, A. R. Rouse, A. Tanbakuchi, M. A. Brewer, R. Sampliner, and A. F. Gmitro, "Confocal microendoscope for use in a clinical setting," Proc. SPIE **6432**, H64320H (2007).
16. P. M. Lane, S. Lam, A. McWilliams, J. C. Leriche, M. W. Anderson, and C. E. MacAulay, "Confocal fluorescence microendoscopy of bronchial epithelium," J Biomed. Opt. **14**, 024008 (2009).
17. K. B. Sung, C. N. Liang, M. Descour, T. Collier, M. Follen, and R. Richards-Kortum, "Fiber-optic confocal reflectance microscope with miniature objective for in vivo imaging of human tissues," IEEE Trans. Biomed. Eng. **49**, 1168–1172 (2002).
18. P. M. Lane, A. L. P. Dlugan, R. Richards-Kortum, and C. E. MacAulay, "Fiber-optic confocal microscopy using a spatial light modulator," Opt. Lett. **25**, 1780–1782 (2000).
19. K. B. Sung, C. Liang, M. Descour, T. Collier, M. Follen, A. Malpica, and R. Richards-Kortum, "Near real time in vivo fibre optic confocal microscopy: subcellular structure resolved," J. Microsc. **208**, 75–75 (2002).
20. A. W. Snyder and J. D. Love, *Optical Waveguide Theory* (Chapman and Hall, 1983).
21. K. L. Reichenbach and C. Xu, "Numerical analysis of light propagation in image fibers or coherent fiber bundles," Opt. Express **15**, 2151–2165 (2007).
22. X. P. Chen, K. L. Reichenbach, and C. Xu, "Experimental and theoretical analysis of core-to-core coupling on fiber bundle imaging," Opt. Express **16**, 21598–21607 (2008).
23. R. Conde, C. Depeursinge, B. Gisin, N. Gisin, and B. Groebli, "Refractive index profile and geometry measurements in multicore fibres," J. Opt. A Pure Appl. Opt. **5**, 269–274 (1996).
24. P. Lane, "Reflection-contrast limit of fiber-optic image guides," J Biomed. Opt. (to be published).
25. N. Kuwamura, Sumitomo Electric USA, Inc. (personal communication, 2009).
26. J. A. Udovich, N. D. Kirkpatrick, A. Kano, A. Tanbakuchi, U. Utzinger, and A. F. Gmitro, "Spectral background and transmission characteristics of fiber optic imaging bundles," Appl. Opt. **47**, 4560–4568 (2008).
27. Y. W. Ma and L. Huang, "The crosstalk study of order-packed flexible image bundles," Proc. SPIE **3552**, 232–237 (1998).